Impact, absorption and evaporation of raindrops on building facades

Abuku, Masaru; Janssen, Hans; Poesen, Jean; Roels, Staf

Published in:
Building and Environment

Link to article, DOI:
10.1016/j.buildenv.2008.02.001

Publication date:
2009

Postprint: Abuku M, Janssen H, Poesen J, Roels S, 2009. Impact, absorption and evaporation of raindrops on building facades, Building and Environment, 44: 113-124.
doi:10.1016/j.buildenv.2008.02.001

Impact, absorption and evaporation of raindrops on building facades

Masaru Abuku [a, *], Hans Janssen [b], Jean Poesen [c], Staf Roels [a]

[a] *Laboratory of Building Physics, Department of Civil Engineering, Katholieke Universiteit Leuven, Kasteelpark Arenberg 40, 3001 Leuven, Belgium*
[b] *Department of Civil Engineering, Technical University of Denmark, Brovej - Building 118, 2800 Kgs. Lyngby, Denmark*
[c] *Physical and Regional Geography Research Group, Katholieke Universiteit Leuven, Celestijnenlaan 200 E, 3001 Leuven, Belgium*
** Corresponding author: Masaru Abuku, Tel: +32 16 321348, Fax: +32 16 321980*
E-mail: masaru.abuku@bwk.kuleuven.be

Abstract: In this paper, the impact, absorption and evaporation of raindrops on building facades is investigated by experimental and numerical means. Laboratory experiments were carried out to study the impact of water drops with different diameters, impact speeds and impact angles on a porous building material surface (ceramic brick). The measurements showed that large drops with high impact speeds splash, and that drops with high impact speeds and small impact angles bounce. The measurements, furthermore, allowed measuring the maximum spreading length and width of the drops as a function of drop diameter, impact speed and impact angle. Then, a numerical analysis was performed to study the distribution of impact speed and angle for raindrops hitting the facade of a $4\times4\times10$ m^3 tower building. The results demonstrated typical and important tendencies of impact angle and speed across the facade. Finally, the experimental and numerical data were used in a more precise three-dimensional simulation of impact, absorption and evaporation of random and discrete wind-driven raindrops. This was compared with the common one-dimensional simulation of absorption and evaporation at the facade considering a continuous uniform rain load as boundary condition, and significant differences between the two approaches were observed.

Keywords: wind-driven rain, raindrop impact, absorption, evaporation, moisture transfer, building facade

Nomenclature

C_s	roughness constant (-)
d	raindrop diameter (mm)
g_m	moisture flux at the wall surface (kg/m^{2}s)
I_h	horizontal rainfall intensity (mm/h)
I_{WDR}	wind-driven rain intensity on a building facade (mm/h)
k	moisture permeability (s) for p_c gradients
k_S	equivalent sand-grain roughness height (m)
l_s	maximum spreading length (mm)
p	vapour pressure (Pa)
p_c	capillary pressure (Pa)
U_{10}	reference wind speed at 10 m above the ground (m/s)
v_i	impact speed (m/s)
w_s	maximum spreading width (mm)
x, y, z	coordinates (m)
x'	position of the external wall surface (m)
y_0	aerodynamic roughness length (m)

Greek symbols

β	surface film coefficient (s^{-1})
ϕ_i	inner diameter of a hypodermic needle or a pipette (mm)
θ_i	impact angle (°)

Subscripts

e	external
s	surface value

1. Introduction

Wind-driven rain (WDR) is one of the most important moisture sources for building facades and has thus been of great concern in building science [1,2]. The behaviour of WDR is governed by the combined effects of the airflow around the building, the geometry of the building and its surroundings, and the horizontal rainfall intensity. In reality the WDR load on building facades is the impingement of individual raindrops whose spatial and temporal distribution is discrete and random. As a matter of fact, WDR is such a complicated boundary condition that in numerical simulations of heat and moisture transfer in building components, it is commonly implemented as a moisture flux averaged over space and time: over the surface area and over the time step of (hourly) climate data [e.g. 3,4]. This is a simplified approach which allows a speedy numerical simulation, but does not correspond to reality. Such simplification of raindrop loads may lead to a significant difference between the model and the reality: e.g. the wet spots caused by individual raindrops hitting the wall surface have a much higher vapour pressure than the averaged surface vapour pressure in the simplified approach. Also when a raindrop splashes or bounces at the wall surface, a fraction of the raindrop is neither absorbed into the wall nor evaporates at the wall surface.

The phenomenon of drop impact has been studied by scientists and engineers in several research fields, and reviews of this topic have been made from different points of view: the reviews of Bennett and Poulikakos [5] and Healy et al. [6] focus on a semi-empirical model to estimate the maximal spreading of a droplet impacting on a solid surface; Rein [7] made a comprehensive review of the liquid drop impact on solid and liquid surfaces and Yarin [8] reviewed the recent advances. Also much research, via numerical modelling and simulation of drop impact, has targeted a better understanding of the detailed behaviour of a droplet at its impact. Recently obtained simulation results demonstrate their noticeable validity [9]. So far however, while the impact of a water drop on a solid surface (e.g. glass surface, steel etc.) has been intensively investigated experimentally and numerically, only few researches have studied drop impact on porous materials [10-12]. The latter publications show that the behaviour of a drop, at impact on a porous material, depends on droplet diameter, impact speed, impact angle, viscosity, surface tension, temperature, material properties etc. Because a raindrop is generally considered as pure liquid water, viscosity and surface tension can be reasonably assumed constant under the temperature and pressure of the liquid phase of water, and are not of interest for this study. The current study focuses on the absorption and evaporation of multiple drops after their impacts as is the fact in driving rain loads on building facades.

The first part of this study focuses on the raindrop impact on a porous building wall surface (ceramic brick). In laboratory experiments, the behaviour of water drops when hitting the building material surface is investigated for droplets with different diameters, impact speeds and impact angles. In the second part, these data are combined with numerical investigations of impact speed, impact angle and specific catch ratio that can be expected for raindrops hitting the facade of a tower building (the catch ratio is the ratio of rainfall intensity collected on a vertical facade to the rainfall intensity on a horizontal surface in the free field; “specific” means that the catch ratio is determined for raindrops with a certain diameter). This part is based on recent advances in computational fluid dynamics, which make it possible to predict the airflow around a building and simulate the trajectories of raindrops around the building, providing a much more reliable and precise distribution of the catch ratio over the building facade [2]. Finally, in a third part, the standard simplified approach, a one-dimensional simulation considering a spatially and temporally averaged rain impact as boundary condition, is compared with a precise three dimensional simulation of the discrete and random raindrop load.

2. Measurement of water drop impact on a porous building material surface

The behaviour of a liquid drop at and after its impact on a porous building material consists of spreading, splashing, bouncing, absorption, evaporation, etc. The definitions of spreading, splashing and bouncing in this paper are illustrated in Fig. 1 based on the figure in Rein [7]. Compared to spreading, splashing or bouncing, phenomena that happen in a few milliseconds, absorption of the droplet by the porous material and the simultaneous evaporation are considered to last at least 100 times longer. The measurements shown here investigate experimentally how a water drop behaves in the first milliseconds after its impact and to what shape it is transformed after spreading. Specifically the maximal spreading length and width are discussed. This data will be used in §4 as input for the discrete three-dimensional simulations of the absorption and evaporation of WDR on building envelopes.

2.1 Measurement set-up

The impact of water drops on a ceramic brick surface was measured in the laboratory. For the material properties of the ceramic brick used in this study, the reader is referred to Hagentoft et al. [4]. For the experiment a specimen was cut out of a fired clay brick, resulting in a smooth surface as shown in Fig. 3 and Fig. 4. Note however that no physical data concerning the surface roughness are available. The drops, with diameters of 2.0 mm (±0.1 mm) and 3.9 mm (±0.1 mm), were released from a hypodermic needle or a pipette placed at different heights, hence with different impact speeds, and at several impact angles. The diameter, impact speed and impact angle were determined from high speed camera (MotionXtra HG-100K, Redlake) images (1000 pictures per second). At the same time, the shape of the wet spot on the surface (the adherence shape of the water drop) was captured with a digital camera. Fig. 2 shows a schematic overview of the measurement set-up.

2.2 Results and discussion

As an example, Fig. 3 and 4 show some pictures of the spots wetted when the water drop spread, spread and splashed, or spread and bounced on the brick surface. In each figure, the wet spots for 4 different impact angles are compared, in Fig. 3 for 2.0 mm drops falling at 6.8 m/s and in Fig. 4 for 3.9 mm drops at 7.5 m/s. Apart from spreading, splashing and bouncing were observed. Splashing was observed for the larger drops (3.9 mm). Bouncing was observed for drops with a low impact angle (24.5º for the 2 mm drops and 15.0º for the 3.9 mm drops). Though it is difficult to determine from the pictures what volume of water bounced and splashed, the observed splashing and bouncing indicate that the volume of rain during a certain period, which is typically measured by a wall mounted rain gauge [2], can be different from the volume of rain acting as a moisture source for the building wall. The wall mounted gauge collects most of the raindrops which may sometimes splash or bounce at porous building wall surfaces, although part of the collected rain can be adhered to the surface and evaporate as well.

Fig. 5 plots the measured maximum spreading length and width of the different drops as a function of impact angle. Each symbol in Fig. 5 represents data of a single drop. Note that, when looking at Fig. 4, the wet spots are sometimes irregularly shaped, making an exact definition of spreading length and width unclear. Here, the maximum spreading length and width of wet parts were determined by taking the middle of the fingering parts (irregularly shaped edges of wet spots as clearly seen in Fig. 4 (a) and (b)). In general the spreading length (Fig. 5 (a)) remains almost constant when the impact angle is above a threshold value and it increases with a decrease of impact angle once below this threshold. But the spreading length of 2.0 mm drops at 6.8 m/s impact speed decreases between 33.3º and 24.5º impact angle due to bouncing. On the other hand, the spreading length of the 3.9 mm drop with an impact angle of 15º is still longer than the one with 38.0º, although the former drop bounced and the latter drop splashed. The spreading length of a 2.0 mm drop at an impact speed of 2.0 m/s remains almost the same when the impact angle is larger than 21.0º and steeply increased with the decrease of impact angle from 21.0º to 10.5º.

The spreading width of the corresponding drops is shown in Fig. 5 (b). The spreading width for a given drop diameter and impact speed slightly increases with an increase of impact angle as a general trend. This relation between the spreading width and the impact angle is almost linear. Yet the spreading width of the three drops that bounced is distinctly smaller than that of the drops with a larger impact angle. Note that each data point in Fig. 5 represents a single drop, but the smooth trends seem to suggest little scatter.

3. Numerical determination of the impact speed, impact angle and size distribution of raindrops at a building facade

The measurements described in the previous section showed that the behaviour of a raindrop at its impact on the ceramic brick surface under study is mainly determined by the size, impact speed and impact angle of the drop. During a natural rain event, impact speeds and angles of rain drops are determined by the trajectory from sky to building facade and will strongly depend on the size of the raindrops, the airflow around the building and the geometry of the building. This section numerically investigates the distribution of these parameters on the facade of a tower shaped building with overall dimensions of $4\times4\times10$ m³.

3.1 Description of the numerical method

The size of raindrops falling in a stagnant air is distributed and its distribution depends on the horizontal rainfall intensity. Although the size distribution of raindrops can not be generalised as a function of horizontal rainfall intensity, the measurements of Best [13] are often used as the most general relation between the size distribution and the horizontal rainfall intensity. The speed of these falling raindrops depends on the size of the raindrop and reaches a certain terminal value while falling. This terminal speed for a given raindrop diameter was given by Best [14] and empirically modelled by Gunn and Kinzer [15]. In the situation that raindrops fall near to an obstacle such as buildings or hills, the size distribution and terminal speed are strongly influenced by the airflow patterns around the obstacle. Choi [16] proposed a numerical simulation of the distribution of raindrops on the surface of such obstacles to determine wind-driven rain loads on building facades; Blocken and Carmeliet [17,18] validated this method on a full scale test building. The method of Choi can be also used to determine the impact speed and impact angle of raindrops for a given diameter and for a given location on the facade. The procedure comprises 3 steps:

(1) the steady-state airflow pattern around the building is calculated with computational fluid dynamics;
(2) raindrop trajectories are obtained by injecting raindrops of different sizes in the calculated airflow pattern and solving their equations of motion;
(3) the impact speed, impact angle and catch ratio of raindrops with a specific diameter are determined based on the calculated raindrop trajectories.

In the calculation of the raindrop trajectory, the turbulent dispersion of raindrops remains an issue of disagreement amongst researchers. Other limitations of wind-driven rain simulation are discussed in Blocken and Carmeliet [17]. Although the validation of Blocken and Carmeliet clearly proved that an accurate determination of the wind-driven rain distribution on building facades can be performed [18], the specific determination of raindrop trajectories still remains to be validated. Especially the trajectories of small raindrops are strongly influenced by the wind, but their effect is less important in the validation of wind-driven rain simulations, especially for moderate to high rainfall intensity.

3.2 Determination of the distribution of impact speed, impact angle and specific catch ratio on the façade of a tower building

Numerical simulation of raindrop trajectories hitting the facade of a tower of $4(x)\times4(y)\times10(z)$ m^3 with wind perpendicular to the facade was conducted with the method of Choi [16]. For different wind speeds the spatial distribution of the impact speed, impact angle and size distribution of raindrops on the facades is investigated. Although the accuracy of the above-mentioned method is not validated for the calculation of impact angle and speed of raindrops, the simulation demonstrated here is considered to be accurate enough to have an overall picture of the distribution of impact angle and speed across the facade.

First, simulation of the airflow field was performed with Fluent 6.2.16. A computational domain with overall dimensions $404(x)\times204(y)\times110(z)$ m^3, in which the centre of the tower is placed at x=202 m and y=102 m on the ground level, was subdivided with 2.1 million tetrahedral cells based on grid sensitivity analysis. The aerodynamic roughness length y_0 to generate the profile of the wind speed, turbulence energy, and energy dissipation rate at the inlet (x= 0 m) was set at 0.1 (m) and the profile of wind speed, turbulence energy, and energy dissipation rate at the upstream part of the computational domain (x=0~150 m) and at the downstream part (x=254~404 m) was treated by use of the wall function with the equivalent sand-grain roughness height k_S= 0.098 (m) and the roughness constant C_s= 10 (-) [19]. At the outlet of the domain, an "outflow boundary condition" was used, in which no streamwise gradient is assumed. At the top and the sides of the domain, symmetric boundary conditions were used. With these conditions, the 3D Reynolds-averaged Navier-Stokes (RANS) equations and the continuity equation were solved using the control volume method. Closure was obtained with use of the realizable k-ε model. The SIMPLE algorithm was used for the pressure-velocity coupling. Pressure interpolation was second order. A second order discretisation scheme was used for all the convection and viscous terms. Note that the use of the tetrahedral mesh causes less accurate prediction especially in the recirculation zone behind the building, but a comparison of its result to the one of a structural mesh with 1.78 million cells showed the airflow facing to the tower is accurately enough predicted with the tetrahedral mesh.

In the next step, the trajectory of raindrops with a diameter of 0.3, 0.4, 0.5, 0.6, 0.7, 0.8, 0.9, 1.0, 1.2, 1.4, 1.6, 1.8, 2.0, 3.0, 4.0, 5.0 and 6.0 mm was simulated with the method of Choi [16]. But now, not only the specific catch ratio, typically needed to determine the wind-driven rain load on building facades, but also the impact speed and angle distribution were calculated. Fig. 6 shows an example of the numerically determined impact angle, impact speed and specific catch ratio of raindrops at the centre (x=200 m, y=102 m, z=0.2~9.8 m) on the facade of the tower. Fig. 6 (a), (c) and (e) show the results simulated with a

reference wind speed U_{10} of 4m/s (U_{10} taken at 10 m height above the ground level); Fig. 6 (b), (d) and (f) with U_{10}=8 m/s.

Fig. 6 (a) and (b) show that the impact angle increases along the height of the tower. The smaller the raindrop size, the more widely distributed the impact angle. The impact angle at a low position simply increases with an increase of drop diameter, the one at a high position first increases and then decreases with increasing drop diameter. Also, the higher the wind speed, the higher the impact angle. Fig. 6 (c) and (d) show the impact speed. The figures illustrate that the spatial distribution of impact speed for a given diameter is not so large. Combining both figures, it can be seen that the impact speed of a small raindrop decreases with an increase of the impact angle. Fig. 6 (e) and (f) show the specific catch ratio for a given drop diameter and position. The smaller the raindrop size, the more widely distributed the specific catch ratio. The position where the specific catch ratio is large also has a large impact angle. In this respect the raindrop impact with a large impact angle is more important as a moisture load than the one with a small impact angle.

4. Validity of the implementation of WDR as boundary condition in numerical models

In this section the commonly used simplified approach in hygrothermal building envelope models to implement WDR as a continuous and uniform boundary flux is compared to a precise three-dimensional simulation taking into account the discrete and random impact of individual raindrops. The input for the latter model is based on the results obtained in the previous two sections. First the two numerical models are described more in detail. Then both models are applied to two rain events and the differences between the obtained simulation results are discussed.

4.1 Traditional model for the implementation of WDR as boundary condition

In most hygrothermal building envelope models, the moisture stress due to WDR on a vertical wall is typically simulated with the assumption of the WDR load spatially averaged over the material surface and temporally averaged over a certain period. Without runoff, the moisture flux at the wall surface g_m can be expressed as [e.g. 20,21]:

$$g_m\big|_{x=+x'} = -\beta\left(p_e - p_s\right) - I_{WDR} \tag{1}$$

$$g_m\big|_{x=-x'} = -k\left.\frac{\partial p_c(x)}{\partial x}\right|_{x=-x'} \tag{2}$$

Here, x is a coordinate with positive direction from the internal to the external, x' is the position of the external wall surface, β is the surface film coefficient, p_e is the vapour pressure of the air adjacent to the external wall surface, p_s is the vapour pressure at the external wall surface, I_{WDR} is the source term of the moisture due to WDR, k is the moisture permeability and p_c is the capillary pressure.

I_{WDR} can be obtained based on climatic data files and standard procedures [1,2] or numerically with the aid of computational fluid dynamics (CFD) and the previously described method of Choi [16] and its extension to deal with climatic data sets by Blocken and Carmeliet [17,18]. In this case, the trajectory of raindrops with a specific diameter is determined in the airflow field calculated with CFD. The specific catch ratio on a certain position of the facade for raindrops with a specific diameter is deduced from the trajectory of raindrops. The specific catch ratio data are averaged into a global catch ratio taking into account the raindrop size distribution [13]. Given the wind speed, wind direction and horizontal rainfall around the building, the WDR intensity I_{WDR} at building facades can then be quantified.

Note that, when the wall surface is saturated, Eqs. (1) and (2) are commonly transformed into:

$$g_m\big|_{x=+x'} = -\beta\left(p_e - p_s\right) \tag{3}$$

$$g_m\big|_{x=-x'} = -k\left(\left.\frac{\partial p_c(x)}{\partial x}\right|_{x=-x'}\right)_{p_c(x')=0} \tag{4}$$

while the excess water due to WDR is mostly considered to disappear from the system as surface runoff. This simple modelling approach (Eqs. (1-4)) has the advantage of an easy and speedy simulation, but its validity is uncertain.

4.2 Discrete model of WDR load on building enclosures

In the discrete model, the random spatial and temporal distribution of impinging raindrops, satisfying the statistical character of the WDR load, can be taken into account. To do so the WDR amount is distributed into a number of raindrops and each raindrop impinges on a certain position on the wall at a certain time. This approach is more realistic than the classical one, but intrinsically requires a three-dimensional simulation of the moisture or the heat and moisture transfer in the material. Of course, for practical cases this results in unacceptably time-consuming simulations, but here such simulation is employed to check the validity of the classical simplified approach.
The discrete model generates a number of spatially and temporally discrete raindrops by use of a random generator. In the current simulations, the random number generator of Compaq Visual Fortran Professional Edition 6.6a was used. The procedure is as follows:

(1) the (global) horizontal rainfall intensity is transformed into specific horizontal rainfall intensities (rainfall intensity for a certain range of raindrop diameter) by use of the Best relation [13];
(2) the specific horizontal rainfall intensity is transformed into the specific wind-driven rain intensity by use of the specific catch ratio;
(3) the specific wind-driven rain which is still spatially and temporally averaged is transformed into specific raindrops randomly falling at a certain time onto a certain location by use of a random generator.

For the current study the specific catch ratio data for a reference wind speed of 4 m/s at 9.8 m above the ground at the centre on the facade of the tower building is used (see the bold line in Fig. 6 (e)). With these catch ratio data, two fictitious 90-minute rain events, with horizontal rainfall intensities 0.1 and 0.5 mm/h, were transformed into raindrop sequences (I_{WDR} =0.062 and 0.345 mm/h) in the above-mentioned way. To investigate the effect of both absorption and evaporation, the rain schedule of the 90 minutes starts with a rain period of 20 minutes, followed by a dry period of 10 minutes, again 20 minutes of rain and finally a dry period during the last 40 minutes. Fig. 7 shows the time course of the diameters of the numerically generated 92 and 292 raindrops which are randomly falling at a certain moment onto a certain location on a material surface with an area of 180mm^2. Note that the load of these raindrops is quantitatively equal to the temporally and spatially averaged WDR load with the intensity of 0.062 and 0.345 mm/h respectively.

Based on Fig. 5 (a) and (b) it can be concluded that due to the corresponding impact angle and speed (see the bold lines in Fig. 6 (a) and (c)) of the raindrops generated (< 1.7 mm as shown in Fig. 7) no splashing or bouncing of impinging raindrops will occur. So only spreading occurs and in the current model a raindrop impinging at the building facade is transformed into an infinitely thin water film with volume and mass of the raindrop and with a rectangular effective surface area for absorption and evaporation, described by the maximum spreading length l_s and spreading width w_s. Although this transformation allows an easier generation of a better mesh, the difference between a real shape and the transformed shape may have some influence on the results in this section. However it is considered that the insights from the simulation results presented below still remain valid. Under isothermal conditions, the viscosity and surface tension can be considered constant and spreading length and width can be modeled as a function of the droplet diameter d, impact speed v_i and impact angle θ_i. Based on Fig. 6 (a), only impact angles larger than 30° are expected in the current study. Therefore the equations of l_s and w_s were made based on the measured data for water drops hitting the ceramic brick surface with impact angles larger than 30°:

$$l_s = 6.1 \times \left(\frac{d^3}{0.127d + 0.209} \right)^{0.5} \times \left\{ 1 - \frac{1.49}{\left(v_i + 4.9 \right)^{0.36}} \right\} \times \left\{ 1 + 0.24 \left(\frac{\theta_i}{90} + 0.51 \right)^{-10} \right\} \tag{5}$$

$$w_s = 4.6 \times \left(\frac{d^3}{0.127d + 0.209} \right)^{0.5} \times \left\{ 1 - \frac{1.49}{\left(v_i + 4.9 \right)^{0.36}} \right\} \times \left\{ 1 + 0.31 \left(\frac{\theta_i}{90} \right) \right\} \tag{6}$$

Each equation was made based on the 13 measurement data. Note that, because no theoretical study of empirical equations of maximum spreading length and spreading width is seen for oblique drop impact on porous materials, arbitrary forms of function were chosen for both equations. However d^3 in both equations represents that l_s and w_s are dependent on the volume of a drop. A comparison of l_s (mm) and w_s (mm) as a function of the impact angle given by Eqs. (5) and (6) with the measurement data is shown in Fig. 8. Note that these equations are only valid for θ_i>30 °, because l_s and w_s for θ_i<30 ° are often very different from the Eqs. (5) and (6) due to splashing and bouncing. Though the equations were not validated for d<2.0 mm, a possible deviation of the equations from the real value is considered to be less significant for smaller raindrops, because the value itself of l_s and w_s of small raindrops is not so large.

Therefore the Eqs. (5) and (6) are adopted for d<2.0 mm and for a low impact speed of small raindrops in the simulations of this paper. Furthermore the temperature dependency of l_s and w_s is not considered here. Note that Eqs. (5) and (6) were only derived for the type of ceramic brick used in this study. If materials with different surface roughness or porosity are used, these equations may no longer hold.

4.3 Numerical simulation of absorption and evaporation of WDR

The absorption and evaporation for the two fictitious rain events are numerically simulated under isothermal condition (10.8 ºC) by the classical one-dimensional averaging model (1-d model) and the three-dimensional discrete model (3-d model). As in the laboratory experiments, ceramic brick is used in the simulations as facade material. The material properties are taken from a previous international modelling benchmark case [4]. The initial relative humidity of the ceramic brick is set at 75 %. The relative humidity of the moist air on the external side (front side) was kept constant at 75 % and the surface film coefficient for the moisture transfer at the external side was also kept constant at 1.54×10^{-7} kg/m^{2}sPa. All other boundaries were assumed impermeable. The mesh for the simulation of the moisture transfer by the finite element method [21] for the 3-d model is shown in Fig. 9. Note that when the raindrops impacted the wall surface in the discrete simulations, it was assumed that the raindrops immediately spread at the wall surface and the time step was reduced to 10^{-6} s. The following assumptions were also adopted in the discrete simulations:

(1) when a raindrop overlaps a wet spot, the mass of the water at the crossover of two wetted parts becomes the sum of the mass of their crossovers;
(2) a cyclic boundary condition was imposed on determining the position of wet spots: e.g. when a wet spot intersects with an edge of the external material surface, one of the split spots by the edge that is not on the external material surface comes at the edge on the other side.

Fig. 10 compares the simulation results of the 1-d model with the results of the 3-d model. Fig. 10 (a) and (b) show the time evolution of the average moisture contents; Fig. 10 (c) and (d) show the time course of the evaporation rate at the entire wall surface; and Fig. 10 (e) and (f) show the time evolution of the amount of the cumulative WDR for both models, cumulative evaporation for both models, the water in the brick for both models and the total adhered water for the 3-d model. Note that no excess water appeared in the simulations with the 1-d model.

As a general trend the average moisture content of the top layer (1 cm) of the brick increased due to the WDR load during rain events and decreased due to evaporation after them. The raindrops which spread on the brick surface were immediately evaporated or absorbed into the brick interior (Fig. 10 (e) and (f)). A comparison of the two models for each case shows an important difference between the two models.

For the horizontal rainfall intensity of 0.1 mm/h, the average moisture content simulated with the 3-d model was higher than the one with the 1-d model. This difference can be attributed to the evaporation rate at the material surface. Looking at Fig. 10 (c), the evaporation rate at the entire wall surface for the 1-d model was most of the time higher than the one for the 3-d model, even though the evaporation rate at and around the small wet spots for the 3-d model was locally very high. Only when a steep increase of the vapour pressure at and around a wet spot was noticed in the 3-d model, the evaporation rate for the 3-d model became higher than the one for the 1-d model. The difference can be explained more clearly by comparing the amount of evaporated water for the two models in Fig. 10 (e).

For the rain event of 0.5 mm/h, on the contrary, the average moisture content simulated with the 1-d model became approximately 2 times higher at the maximum than the one predicted with the 3-d model. The reason for this is the fact that in the simulation with the 1-d model, the moisture content at the material surface remained below the saturated moisture content and the vapour pressure at the material surface was kept uniformly at a certain relatively low value. On the other hand, in the simulation with the 3-d model, the water of the raindrops quickly spread into the wall inside and evaporated because of the high vapour pressure at and around the wet spots. So for a higher WDR intensity, while the 1-d model allows an easy absorption, maintaining low surface vapour pressure and slow evaporation, the 3-d model yields a locally high absorption and evaporation, sustaining several scattered islands of high vapour pressure at the material surface.

5. Conclusions

The validity of the implementation of wind-driven rain as boundary condition in hygrothermal building envelope models was experimentally and numerically investigated and elaborated in detail.

The first part of this paper experimentally investigated the behaviour of raindrops in a few milliseconds after their impact on building material surfaces: the water drop impact on a porous material's surface (ceramic brick) was measured. The results showed that a drop with a diameter of 3.9 mm splashed at its impact and a drop with a small impact angle and speed bounced. These observations indicate that the volume of the raindrops corrected by a driving rain gauge can differ from the moisture load due to rain on the building facade, because side walls of the gauge may collect a part of the water that has splashed or bounced on the gauge, while part of the raindrops which impact the building facade may not be loaded onto the building facade due to splashing and bouncing. Furthermore splashing and bouncing can be different for facade and gauge surfaces due to different surface phenomena. Also the maximum spreading length and width of raindrops, which are the important parameters for investigating the absorption and evaporation of rain at the building facade, were determined. The spreading length increases with a decrease of impact angle and with an increase of drop diameter and impact speed; the spreading width increases with an increase of impact angle and with an increase of drop diameter and impact speed. Furthermore, the occurrence of bouncing reduces the maximum spreading length and width.

Secondly the impact angle, impact speed and specific catch ratio of the raindrops at the facade of the tower building were numerically determined and some trends were observed:

- the impact angle and specific catch ratio of small raindrops are spatially widely distributed; the ones of large raindrops are spatially rather uniform;
- the impact angle is often large where the specific catch ratio is large;
- the impact speed of all the raindrops is spatially rather uniform regardless of the airflow speed around the building;
- the impact speed of raindrops at the building facade is considerably close to their terminal speed [14, 15];
- the impact angle, impact speed and specific catch ratio on the building facade increases with an increase of the reference wind speed when the cardinal wind is perpendicular to the building facade.

When these findings are confronted with the measurement results of drop impact, for the building studied, the wind-driven rain is more important at a high location on the facade than at a low location, not only because the high location is exposed to more wind-driven rain, but also because a raindrop at the low location has often a small impact angle and thus bounces and is not entirely loaded onto the facade as a moisture source.

Finally the classical spatial and temporal averaging of the WDR load on building enclosures was compared to a precise three-dimensional simulation, in which the discrete impact of individual raindrops was modelled. The average moisture contents simulated in these two ways were quite different. In one case for a horizontal rainfall intensity of 0.1 mm/h, the simulation with the commonly used 1-d model led to an underestimation of the average moisture content due to an overestimation of the evaporation rate. In the other case for 0.5 mm/h, the simulation with the 1-d model led to an overestimation of the average moisture content due to an underestimation of the evaporation rate. Note that, in the current simulations, a part of the kinetic energy of raindrops which forces the water into the wall interior was ignored, though influences of this energy on the absorption might be of some importance.

Acknowledgements

The results in this paper have been obtained within KUL OT/04/28, 'Towards a reliable prediction of the moisture stress on building enclosures', funded by the K.U.Leuven and IWT 050154, 'Heat, air and moisture performance engineering: a whole building approach', funded by the Flemish Government. These financial supports are gratefully acknowledged.

Measurements of drop impact were performed with the high speed camera of the Department of Biosystems, K.U.Leuven. We would like to thank Prof. Ramon and his co-workers for the fruitful collaboration.

References

[1] Sanders C. Heat, air and moisture transfer in insulated envelope parts. IEA Annex 24, Final report – Vol. 2, Task 2: Environmental conditions. Leuven: Acco Leuven; 1996.

[2] Blocken B, Carmeliet J. A review of wind-driven rain research in building science. Journal of Wind Engineering and Industrial Aerodynamics 2004; 92 (13): 1079-1130.

[3] Künzel HM. Verfahren zur ein- und zweidimensionalen Berechnung des gekoppelten Wärme- und Feuchtetransports in Bauteilen mit einfachen Kennwerten. PhD thesis, Universty of Stuttgart; 1994.
[4] Hagentoft CE, Kalagasidis AS, Adl-Zarrabi B, Roels S, Carmeliet J, Hens H, Grunewald J, Funk M, Becker R, Shamir D, Adan O, Brocken H, Kumaran K, Djebbar R. Assessment method of numerical prediction models for combined heat, air and moisture transfer in building components: benchmarks for one-dimensional cases. Journal of thermal envelope and building science 2004; 27 (4): 327-352.
[5] Bennett T, Poulikakos D. Splat-quench solidification: estimating the maximum spreading of a droplet impacting a solid surface. Journal of Materials Science 1993; 28: 963-970.
[6] Healy WM, Hartley JG, Abdel-Khalik SI. Comparison between theoretical models and experimental data for the spreading of liquid droplets impacting a solid surface. International Journal of Heat and Mass Transfer 1996; 39(14): 3079-3082.
[7] Rein M. Phenomena of liquid drop impact on solid and liquid surfaces. Fluid Dynamics Research 1993; 12: 61-93.
[8] Yarin AL. Drop impact dynamics: splashing, spreading receding, bouncing…. Annual Review of Fluid Mechanics 2006; 38: 159-192.
[9] Fujimoto H, Shiotani Y, Tong AY, Hama T, Takuda H. Three-dimensional numerical analysis of the deformation behaviour of droplets impinging onto a solid substrate. International Journal of Multiphase Flow 2007; 33: 317-332.
[10] Alleborn N, Raszillier H, Anthonissen K, Lievens O. Spreading and sorption of a droplet on a porous substrate. In: Schweizer PM, Cohu O. editor. Proceedings of the 5th European Coating Symposium, Advances in Liquid Film Coating Technology, Fribourg, Switzerland; 2003, p. 246-251.
[11] Reis NC, Griffiths RF, Santos JM. Numerical simulation of the impact of liquid droplets on porous surfaces. Journal of Computational Physics 2004; 198: 747-770.
[12] Zadražil A, Stepanek F, Matar OK. Droplet spreading, imbibition and solidification on porous media. Journal of Fluid Mechanics 2006; 562: 1-33.
[13] Best AC. The size distribution of raindrops. Quarterly Journal of the Royal Meteorological Society 1950; 76: 16-36.
[14] Best AC. Empirical formulae for the terminal velocity of water drops falling through the atmosphere. Quarterly Journal of the Royal Meteorological Society 1950; 76: 302-311.
[15] Gunn R, Kinzer GD. The terminal velocity of fall for water droplets in stagnant air. Journal of Meteorology 1949; 6: 243-248.
[16] Choi ECC. Simulation of wind-driven-rain around a building. Journal of Wind Engineering and Industrial Aerodynamics 1993; 46&47: 721-729.
[17] Blocken B, Carmeliet J. Spatial and temporal distribution of wind-driven rain on low-rise building. Wind and Structures 2002; 5 (5): 441-462.
[18] Blocken B, Carmeliet J. Validation of CFD simulations of wind-driven rain on a low-rise building facade. Building and Environment 2007; 42(7): 2530–2548.
[19] Blocken B, Stathopoulos T, Carmeliet J. CFD simulation of the atmospheric boundary layer: wall function problems. Atmospheric Environment 2007; 41: 238-252.
[20] Hall C, Hoff WD. Water transport in brick, stone and concrete. London: Spon Press; 2002.
[21] Janssen H, Blocken B, Carmeliet J. Conservative modelling of the moisture and heat transfer in building components under atmospheric excitation. International Journal of Heat and Mass Transfer 2007; 50: 1128-1140.

Figure Captions

Fig. 1. Definitions of spreading, splashing and bouncing (based on the figure in Rein [7]).

Fig. 2. Schematic overview of the measurement set-up of water drop impact at building material surfaces. ϕ_i: inner diameter [mm] of the needle or the pipette to generate a water drop.

Fig. 3. Pictures of wet spots on ceramic brick surface. Drop diameter: 2.0 mm ($\pm$0.1 mm); impact speed: 6.8 m/s; impact angle: (a) 90.0º, (b) 49.3º, (c) 43.2º and (d) 24.5º. The drop in (d) bounced.

Fig. 4. Pictures of wet spots on ceramic brick surface. Drop diameter: 3.9 mm ($\pm$0.1 mm); impact speed: 7.5 m/s; impact angle: (a) 90.0º, (b) 48.5º, (c) 38.0º and (d) 15.0º. The drops in (a), (b) and (c) splashed. The drop in (d) bounced.

Fig. 5. (a) Spreading length (l_s) and (b) spreading width (w_s) of water drops at a ceramic brick surface. d: drop diameter (mm); v_i: impact speed (m/s); θ_i: impact angle (the minimum angle between the wall and the direction of impact) (º). Each symbol represents data of a single drop. Note that 3 drops bounced and 6 drops splashed.

Fig. 6. Numerically determined (a,c) impact angle, (b,d) impact speed and (e,f) specific catch ratio of raindrops at centre on the facade of the tower. The reference wind direction is perpendicular to the facade. U_{10}=4 m/s for (a), (c) and (e); U_{10}=8 m/s for (b), (d) and (f). The bold lines are used in the simulations of Section 4.

Fig. 7. Time course of the diameter of numerically generated raindrops over the brick wall surface (180 mm^2) on the facade of the tower. (a) I_h=0.1 mm/h (I_{WDR}=0.062 mm/h); (b) I_h=0.5 mm/h (I_{WDR}=0.345 mm/h). Note that there is no rain load from 3000 s to 5400 s.

Fig. 8. (a) Spreading length (l_s) and (b) spreading width (w_s) of water drops at a ceramic brick surface for θ_i >30º. The symbols (□ and ○) show the measurement data. The lines show Eqs. (5) and (6). The lines of raindrops with a diameter of 2.0 and 3.9 mm are compared to the measurement data. The impact speed for the three lines of raindrops with a diameter of 0.3, 0.6 and 1.0 mm is the terminal speed given by Best (1951). d: drop diameter (mm); v_i: impact speed (m/s); θ_i: impact angle (the minimum angle between the wall and the direction of impact) (º).

Fig. 9. Mesh over the material surface for FEM simulation (3D). Total number of nodes in mesh: 4194; number of nodes at the front side: 1701; number of nodes at the back side: 150.

Fig. 10. Simulation results. (a) and (b) Average moisture content in brick; (c) and (d) evaporation rate at the entire surface; (e) and (f) cumulative mass of water. In (a), (c) and (e), I_h=0.1 mm/h and I_{WDR}=0.062 mm/h; in (b), (d) and (f), I_h=0.5 mm/h and I_{WDR}=0.345 mm/h. The dash lines show the results of the 1-d simulations with the classical model for WDR loads; the solid lines show the results of the 3-d simulations with the discrete model for WDR loads.

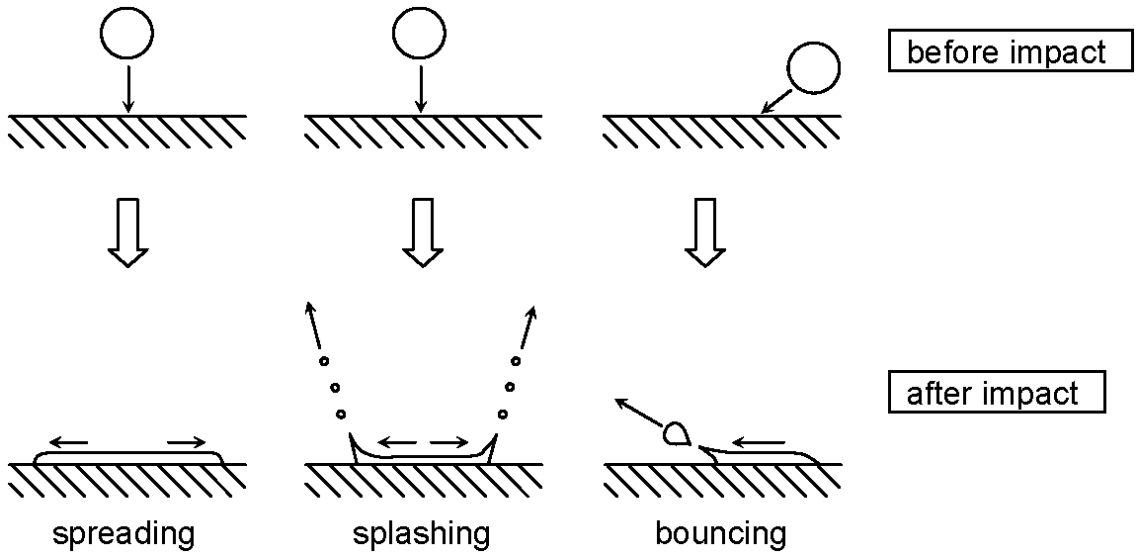

Fig. 1. Definitions of spreading, splashing and bouncing (based on the figure in Rein [7]).

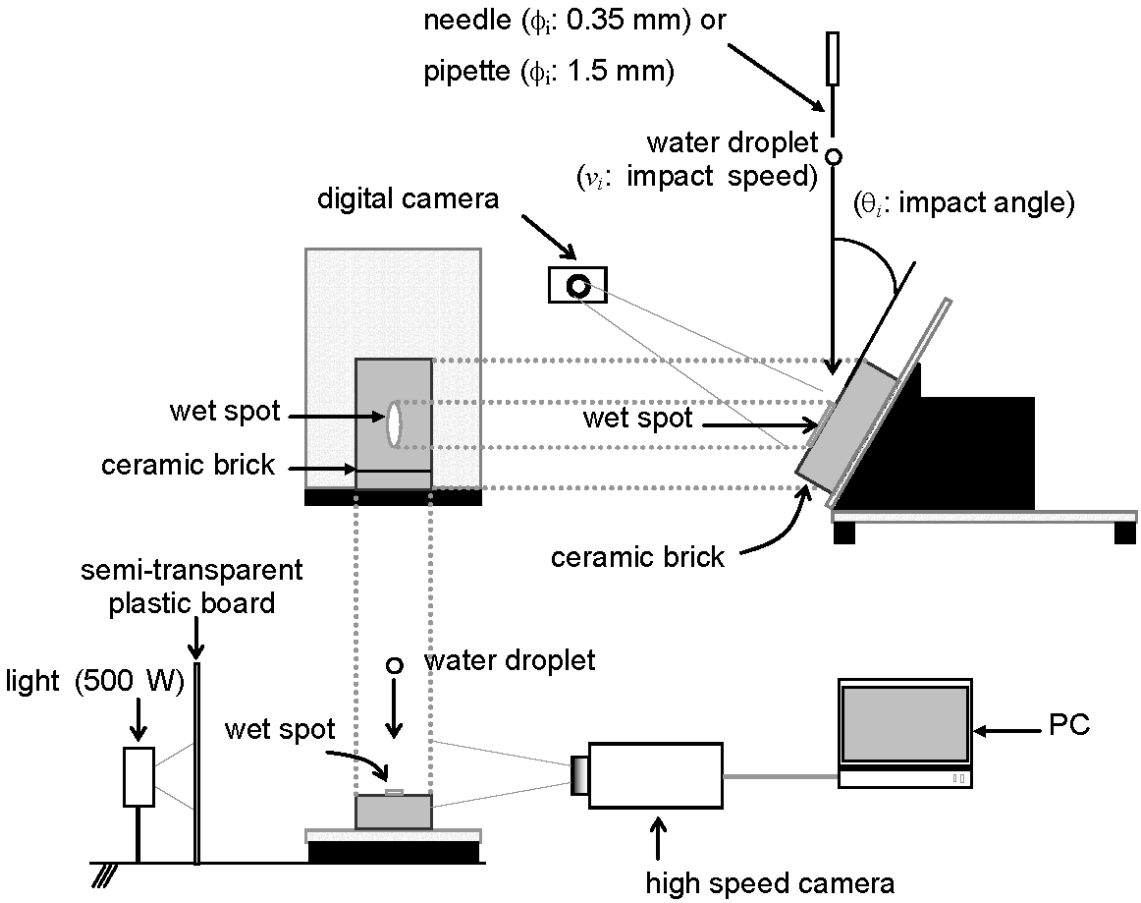

Fig. 2. Schematic overview of the measurement set-up of water drop impact at building material surfaces. ϕ_i: inner diameter [mm] of the needle or the pipette to generate a water drop.

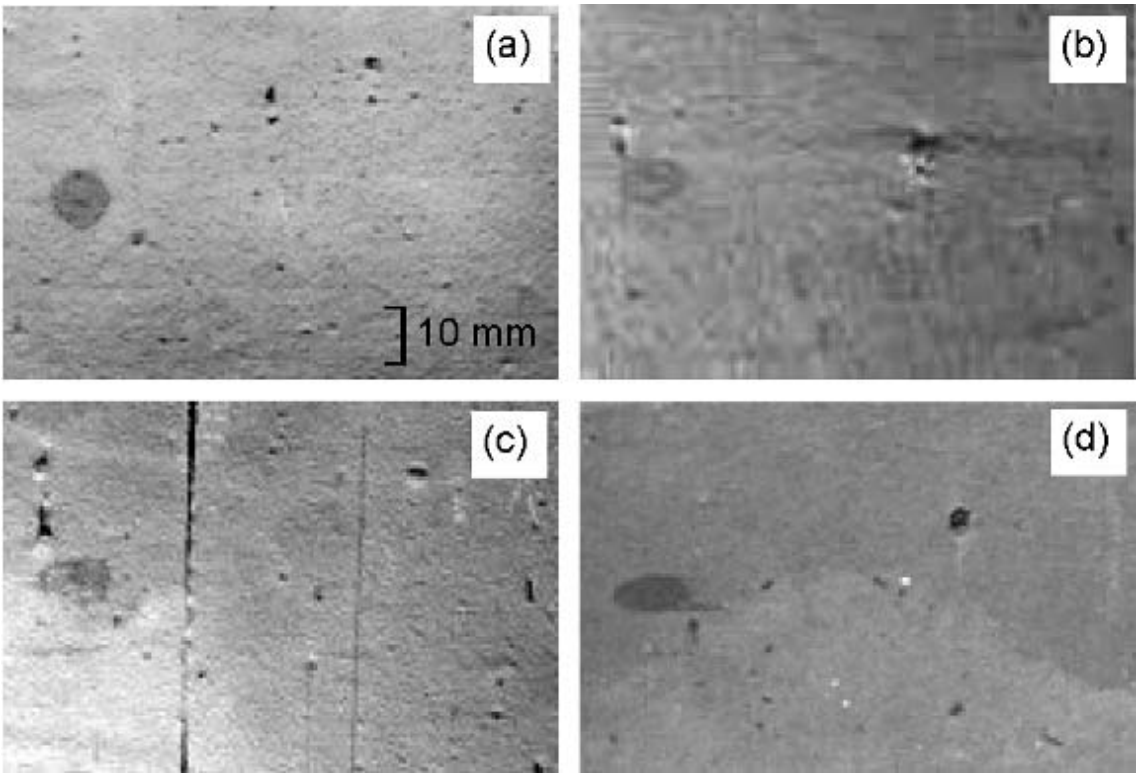

Fig. 3. Pictures of wet spots on ceramic brick surface. Drop diameter: 2.0 mm (±0.1 mm); impact speed: 6.8 m/s; impact angle: (a) 90.0º, (b) 49.3º, (c) 43.2º and (d) 24.5º. The drop in (d) bounced.

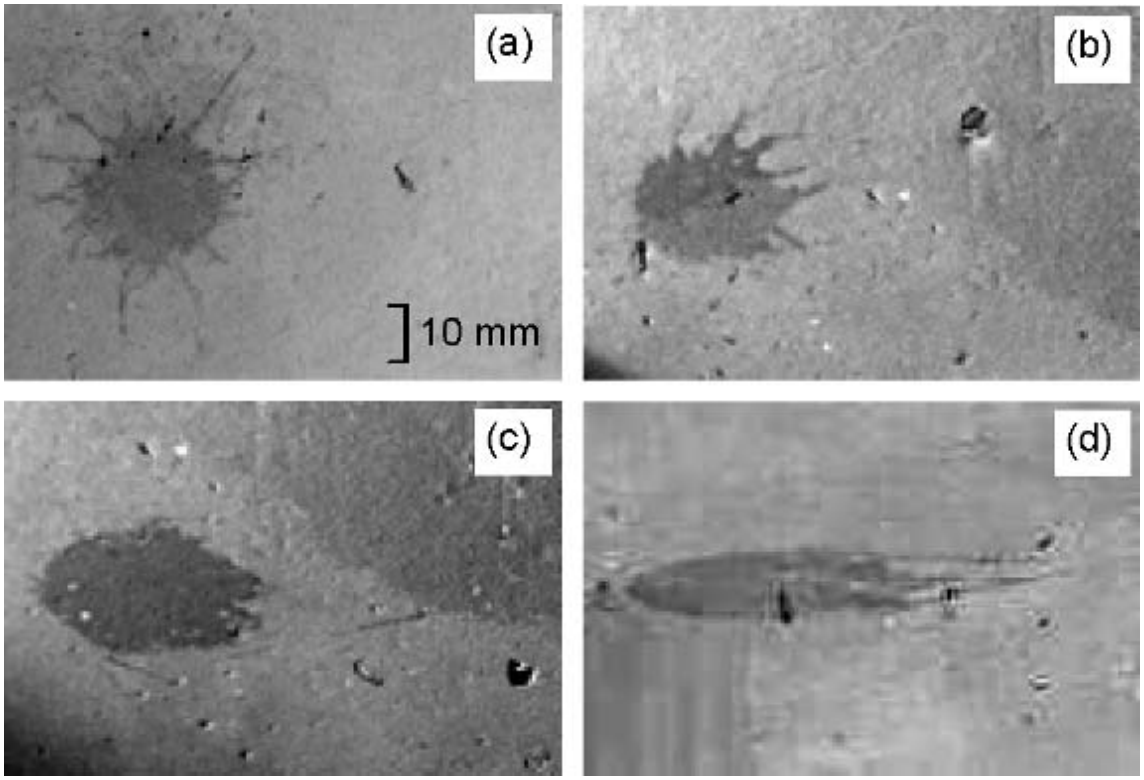

Fig. 4. Pictures of wet spots on ceramic brick surface. Drop diameter: 3.9 mm (±0.1 mm); impact speed: 7.5 m/s; impact angle: (a) 90.0º, (b) 48.5º, (c) 38.0º and (d) 15.0º. The drops in (a), (b) and (c) splashed. The drop in (d) bounced.

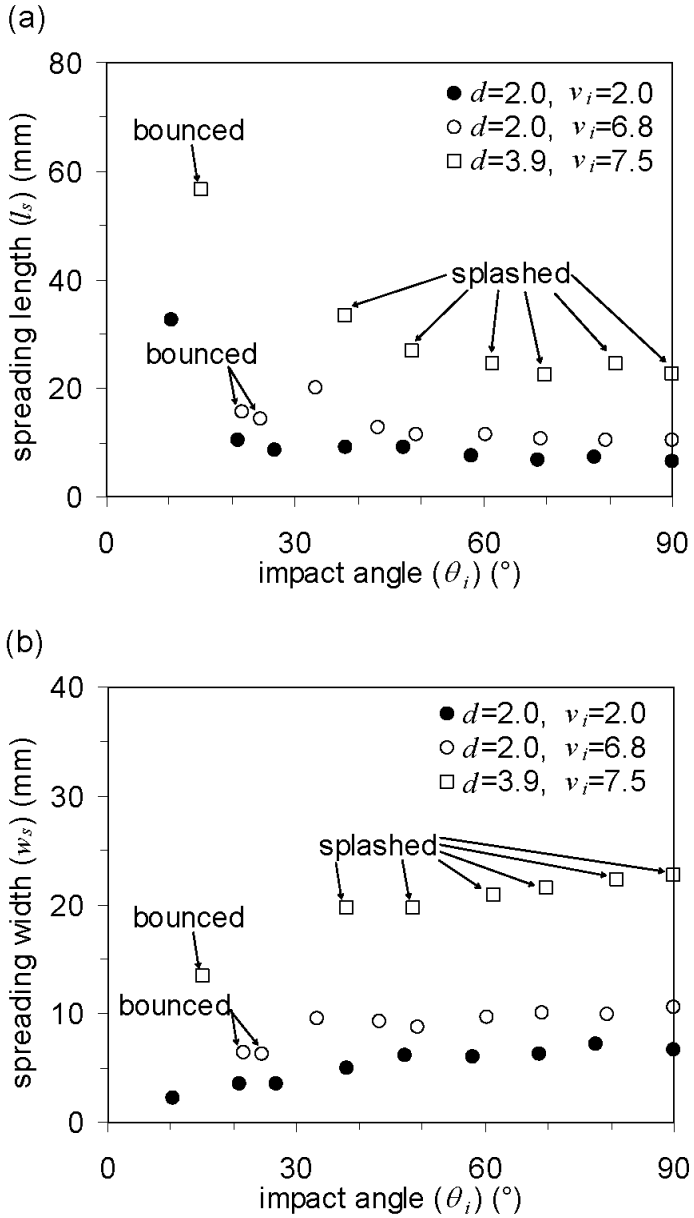

Fig. 5. (a) Spreading length (l_s) and (b) spreading width (w_s) of water drops at a ceramic brick surface. d: drop diameter (mm); v_i: impact speed (m/s); θ_i: impact angle (the minimum angle between the wall and the direction of impact) (º). Each symbol represents data of a single drop. Note that 3 drops bounced and 6 drops splashed.

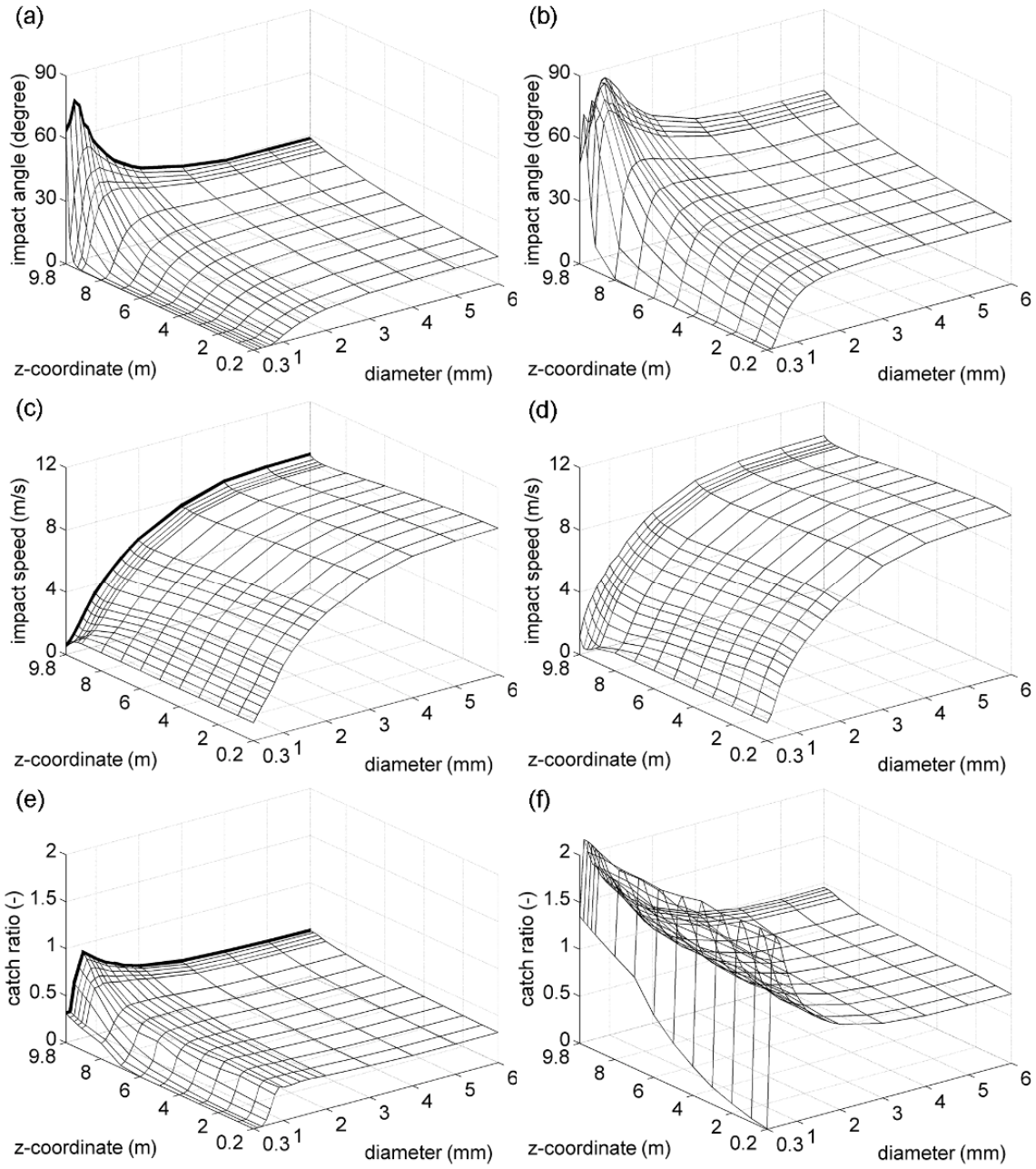

Fig. 6. Numerically determined (a,c) impact angle, (b,d) impact speed and (e,f) specific catch ratio of raindrops at centre on the facade of the tower. The reference wind direction is perpendicular to the facade. U_{10}=4 m/s for (a), (c) and (e); U_{10}=8 m/s for (b), (d) and (f). The bold lines are used in the simulations of Section 4.

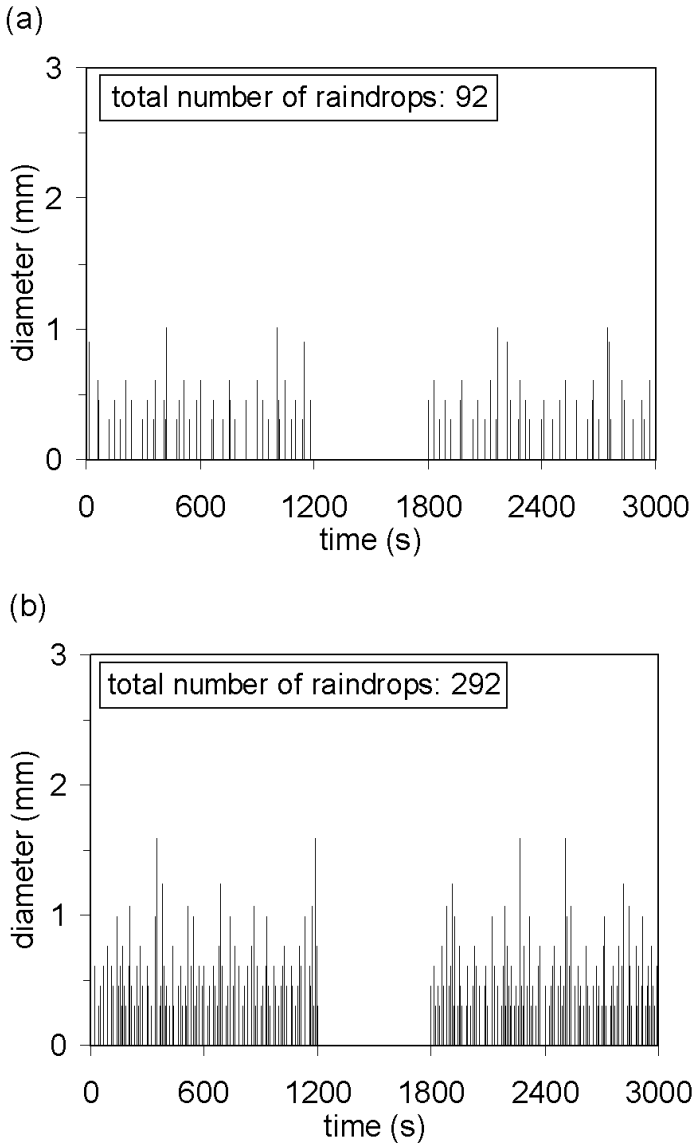

Fig. 7. Time course of the diameter of numerically generated raindrops over the brick wall surface (180 mm^2) on the facade of the tower. (a) I_h=0.1 mm/h (I_{WDR}=0.062 mm/h); (b) I_h=0.5 mm/h (I_{WDR}=0.345 mm/h). Note that there is no rain load from 3000 s to 5400 s.

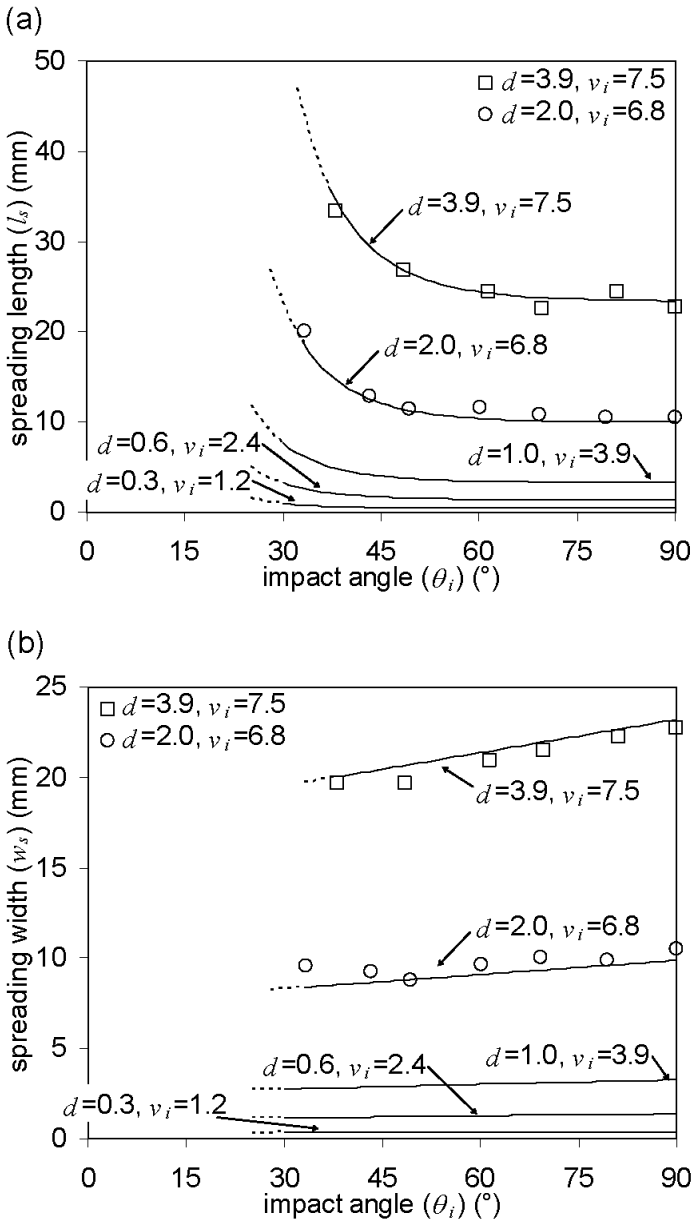

Fig. 8. (a) Spreading length (l_s) and (b) spreading width (w_s) of water drops at a ceramic brick surface for θ_i >30º. The symbols (□ and ○) show the measurement data. The lines show Eqs. (5) and (6). The lines of raindrops with a diameter of 2.0 and 3.9 mm are compared to the measurement data. The impact speed for the three lines of raindrops with a diameter of 0.3, 0.6 and 1.0 mm is the terminal speed given by Best (1951). d: drop diameter (mm); v_i: impact speed (m/s); θ_i: impact angle (the minimum angle between the wall and the direction of impact) (º).

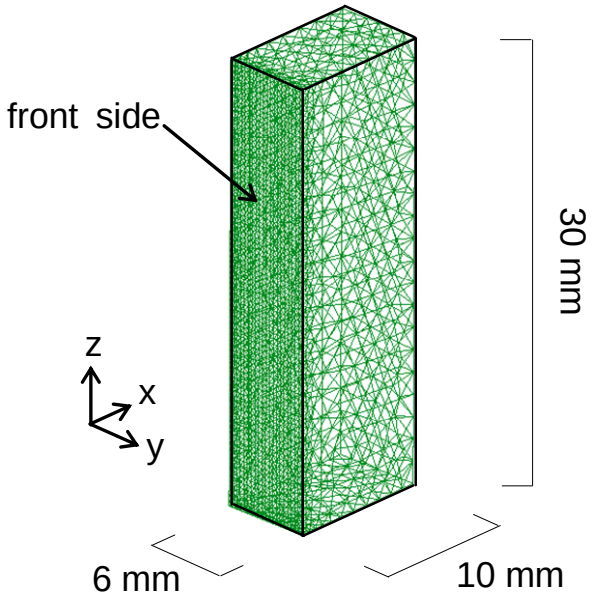

Fig. 9. Mesh over the material surface for FEM simulation (3D). Total number of nodes in mesh: 4194; number of nodes at the front side: 1701; number of nodes at the back side: 150.

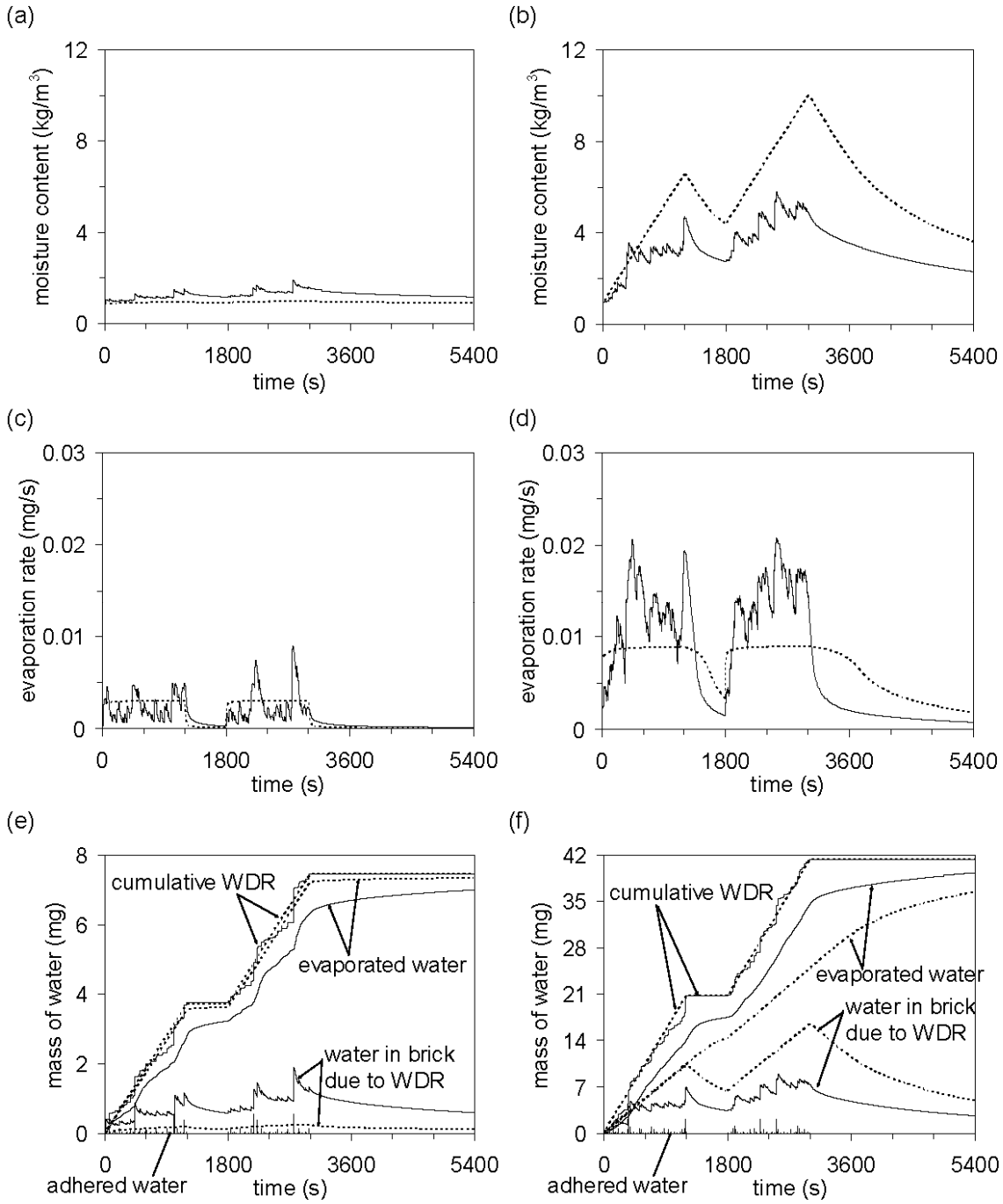

Fig. 10. Simulation results. (a) and (b) Average moisture content in brick; (c) and (d) evaporation rate at the entire surface; (e) and (f) cumulative mass of water. In (a), (c) and (e), I_h=0.1 mm/h and I_{WDR}=0.062 mm/h; in (b), (d) and (f), I_h=0.5 mm/h and I_{WDR}=0.345 mm/h. The dash lines show the results of the 1-d simulations with the classical model for WDR loads; the solid lines show the results of the 3-d simulations with the discrete model for WDR loads.